INORGANIC CHEMISTRY
FRONTIERS

RESEARCH ARTICLE

View Article Online
View Journal | View Issue

Check for updates

Cite this: *Inorg. Chem. Front.*, 2020, **7**, 2478

High performance single-molecule magnets, Orbach or Raman relaxation suppression?†

Alejandro Castro-Alvarez,[a] Yolimar Gil,[b] Leonel Llanos[a] and Daniel Aravena *[a]

Received 27th April 2020,
Accepted 28th May 2020

DOI: 10.1039/d0qi00487a

rsc.li/frontiers-inorganic

The current figure of merit to evaluate Single Molecule Magnet (SMM) performance is the blocking temperature (T_B). The best SMMs show T_B values close to liquid nitrogen boiling point (77 K) while their Orbach effective demagnetization barriers (U_{eff}) are significantly larger, exceeding 2000 K in some cases. As current high performance SMMs approach the axial limit, new strategies to suppress demagnetization by vibrational tuning have been suggested. In this article, we analyse a set of 17 current high performance SMMs to identify which demagnetization mechanism is limiting the blocking temperature. For the best systems (T_B > 50 K), the limiting mechanism is thermally assisted tunneling and the blocking temperature will depend on the exponential parameters U_{eff} and τ_0. Strategies focusing on Raman (vibrational) suppression are expected to have a limited effect for this group. In contrast, systems with lower blocking temperatures (T_B < 50 K) would benefit from such strategies, although they are not expected to surpass current record T_B values. The Orbach limit for the blocking temperature can be conveniently estimated using *ab initio* CASSCF methods. Finally, a recent proposal for a hypothetical high performance SMM is analysed under the presented framework, showing its potential to improve record blocking temperatures.

Published on 01 June 2020. Downloaded on 2/3/2025 9:56:01 AM.

Introduction

Single Molecule Magnets (SMMs) are intensely studied due to their potential application as molecular devices for information storage and processing. Like a bit from a Hard-Disk drive, SMMs can retain their magnetic moment direction in the absence of a magnetic field.[1,2] Unfortunately, magnetic blocking is limited to cryogenic temperatures due to demagnetization mechanisms which induce spin relaxation.

Nowadays, spin dynamics in single molecule magnets is understood as a complex phenomenon,[3–12] occurring by parallel mechanisms involving electronic and vibrational characteristics of the SMM and the interaction with its environment. From the temperature dependence of the relaxation time (τ), three main relaxation regimes are normally observed: (i) a temperature independent region at low temperature, which is associated with quantum tunnelling demagnetization involving only the ground (pseudo-) doublet. (ii) A region displaying power dependence of τ concerning temperature, normally assigned as Raman relaxation and (iii) exponential dependence of τ, commonly observed in the high temperature region. Although this regime is usually associated with Orbach relaxation, it is important to note that other demagnetization mechanisms can also lead to exponential dependence of τ, such as thermally assisted quantum tunnelling.

In a strict sense, Orbach and Raman relaxation refer to two-phonon mechanisms.[13] In the case of Orbach mechanism, one excited state inside the phonon continuum mediates relaxation and yields an exponential dependence of $\tau(T)$. Raman mechanism requires nonzero matrix elements for the crystal potential between relaxing states (first-order Raman) or the existence of a third state connecting them (second-order). State energies from contemporary high-performance SMMs are well above any estimation of the phonon continuum, yet an exponential dependence of $\tau(T)$ is usually observed in the high temperature range. As said earlier, the observation of an exponential regime for $\tau(T)$ does not necessarily imply that the classical Orbach mechanism is the main source of relaxation under these conditions. However, it is common practice to name the exponential regime as Orbach and we follow this convention.

The key parameters related to SMM performance have evolved to account for this complexity. Some years ago, the most important figure of merit for an SMM was the effective demagnetization barrier (U_{eff}), obtained from the fit of the temperature dependence of the relaxation time to an Arrhenius law. In this way, U_{eff} provides information about the

[a]*Departamento de Química de los Materiales, Facultad de Química y Biología, Universidad de Santiago de Chile, Casilla 40, Correo 33, Santiago, Chile. E-mail: daniel.aravena.p@usach.cl*
[b]*Departamento de Química Inorgánica y Analítica, Facultad de Ciencias Químicas y Farmacéuticas, Universidad de Chile, Santiago, Chile*

†Electronic supplementary information (ESI) available. Supplementary tables and computational results for all models; an input example file to calculate tunnelling relaxation times. See DOI: 10.1039/d0qi00487a

This journal is © the Partner Organisations 2020

Published on 01 June 2020. Downloaded on 2/3/2025 9:56:01 AM.

exponential relaxation regime, without consideration of other sources of demagnetization. Currently, a more informative parameter is the blocking temperature (T_B),[14–16] defined as the temperature where relaxation time coincides with the characteristic time of the experiment.[17] There are some variants on the exact definition of T_B: (i) the maximum in the zero-field cooled (ZFC) magnetic susceptibility curve, (ii) the temperature at which τ = 100 s and (iii), the maximum temperature where an open hysteresis is observed.[17]

Nowadays, there is no consensus about the best way to measure the blocking temperature. The definition of T_B with respect to a reference relaxation time (*e.g.* τ_{ref} = 100 s) is transparent but arbitrary at the same time. In principle, a large T_B can be obtained if τ_{ref} is chosen to be fast. The condition of an open hysteresis to set T_B is criticized because this approach is strongly dependent on the field sweep rate. Significantly higher T_B values can be obtained by choosing a fast sweep program. The definition based on ZFC/FC experiments is a popular approach to obtain T_B. However, the blocking temperature measured in this way should be sensitive to the temperature program applied for the measurement.[17] Unfortunately, these technical details are not always present in publications, and it is hard to know how comparable are blocking temperatures from different studies. Despite these complications, T_B displaced U_{eff} as the relevant figure of merit to evaluate SMM performance.

Comparing U_{eff} and T_B values, it is evident that the effective demagnetization barrier is not an accurate predictor of T_B since complexes with similar values of U_{eff} can display strongly dissimilar blocking temperatures.[18] Some of the latest high-performance SMMs surpass 2000 K in their energy barriers, although the record blocking temperature is significantly lower (80 K, determined by hysteresis measurements).[19]

As the Orbach barrier is not the central quantity anymore, new strategies focusing on the suppression of spin-vibration coupling have emerged as alternative ways to improve SMM properties without necessarily rising U_{eff}. Chemical strategies to achieve this objective include ligand stiffening to minimize atomic displacement for the magnetically relevant atoms, symmetry tuning to cancel spin-vibration coupling and detuning of electronic and vibrational energy levels.[20] Another strategy that might influence vibrational displacements is the use of high pressure. However, this effect will be simultaneous to ligand field modification so the vibrational effect is expected to be hard to isolate.[21,22] Commonly, chemical modifications designed for Raman and Orbach suppression will differ. Chemists must decide which strategy is the most promising before embarking in a laborious and resource-consuming synthetic project.

In this article, we analyse a set of 17 literature examples of high-performance SMMs to determine the potential of Raman and Orbach tuning for the rise of their blocking temperatures. We determine which systems are expected to improve by vibrational tuning and which should be more insensitive. *Ab initio* calculations are employed to estimate the Orbach limit for the blocking temperature, showing that current computational methodologies are suitable to provide sensible predictions regarding this parameter. Finally, we analyse a recent proposal for a hypothetical high performance SMM, providing an estimate for its maximum potential blocking temperature.

Results and discussion

Table 1 presents a set of current high performance SMMs, all featuring U_{eff} > 600 K and τ = 100 s blocking temperatures ($T_{B,100}$) ranging from 2 K to 67 K. Some systems have a tunnelling relaxation time faster than 100 s, so T_B cannot be defined and is limited by the tunnelling mechanism. For these cases (**10–14**, **16**, **17**), we define the tunnelling limited blocking temperature T_{QT} = 0, remaining molecules are limited by other mechanisms and thus, T_{QT} = ∞. Equalizing the Raman (CT^n) and Orbach $\left(\exp\left(-\frac{U_{eff}}{T}\right)/\tau_0\right)$ terms to τ^{-1} = 0.01 s^{-1} allows to define the Raman and Orbach limiting temperatures, T_{Ra} and T_{Or}, respectively. Temperature dependent relaxation rate is represented by the expression:

$$\frac{1}{\tau} = \frac{1}{\tau_0}\exp(-U_{eff}/T) + CT^n + \frac{1}{\tau_{QT}} \quad (1)$$

where the tunnelling term is omitted for **6**, **7**, **8** and **15** since τ_{QT} was not fitted in their original publications. Despite the simplicity of this analysis, valuable information can be obtained by comparing the three limiting temperatures. Interestingly, there is no predominant mechanism determining T_B since there are examples where the lowest limiting temperature is associated with tunnelling, Raman and Orbach mechanisms (highlighted in bold).

Importantly, the limiting mechanism for best SMMs (T_B > 50 K, complexes **1**, **2**, **3**, **4**, **7** and **9**) is predominantly Orbach. Even in the cases where $T_{Ra} < T_{Or}$ (*i.e.* complexes **1**, **3** and **9**), the difference between these two parameters is small. Thus, suppression of Raman relaxation will only lead to a modest increase in T_B and tuning of Orbach parameters is necessary to obtain SMMs with higher blocking temperatures. To estimate the maximum increase of $T_{B,100}$ due to complete Raman suppression, we reconstructed the τ^{-1} curve neglecting the Raman term:

$$\frac{1}{\tau} = \frac{1}{\tau_0}\exp(-U_{eff}/T) + \frac{1}{\tau_{QT}} \quad (2)$$

Table 2 shows the "Raman free" blocking temperature ($T_{B,100,noR}$), showing that the increase of the blocking temperature is at most 7 K for T_B > 50 K systems. On the other hand, Raman limited systems are of course sensitive to the suppression of this mechanism and will greatly benefit from vibrational tuning. From the studied systems, **5**, **6**, **8** and **15** featured a maximum increase of T_B of 41 K, 45 K, 32 K and 24 K due to Raman neglection. Despite these significant improvements, $T_{B,100,noR}$ values do not surpass blocking temperatures for the Orbach limited group. In practice, it is unlikely to achieve complete suppression of Raman relaxation. However, even a partial hindrance of this mechanism can sig-

Published on 01 June 2020. Downloaded on 2/3/2025 9:56:01 AM.

Table 1 Relaxation parameters, blocking temperatures, tunnelling, Raman and Orbach limiting temperatures for a set of high-performance SMMs. Experimentally adjusted relaxation parameters (τ_0, U_{eff}, C, n, τ_{QT}) were obtained from corresponding references. $T_{B,100}$ corresponds to the temperature where τ = 100 s. Complexes **10–14**, **16** and **17** do not have $T_{B,100}$ since their tunneling relaxation time is already lower than 100 s. All temperatures are expressed in K

	Chemical formula	U_{eff}/K	τ_0/s	τ_{QT}/s	C/s^{-1} K^{-n}	n	$T_{B,100}$	T_{QT}	T_{Ra}	T_{Or}	Ref.
1	$[Dy(Cp(Me)_5)(Cp(iPr)_5)][B(C_6F_5)_4]$	2217	$4.20\ 10^{-12}$	25 000	$3.10\ 10^{-8}$	3	67	∞	**69**	72	19
2	$[Dy\{Cp(iPr)_4(Me)\}_2][B(C_6F_5)_4]$	2112	$4.01\ 10^{-12}$	2452	$1.57\ 10^{-6}$	2.07	64	∞	69	**68**	23
3	$[Dy\{Cp(iPr)_4(Et)\}_2][B(C_6F_5)_4]$	1986	$7.79\ 10^{-12}$	447	$3.36\ 10^{-8}$	3.02	59	∞	**65**	66	23
4	$[Dy\{Cp(iPr)_5\}_2][B(C_6F_5)_4]$	1922	$1.18\ 10^{-11}$	1187	$8.04\ 10^{-8}$	2.31	65	∞	161	**65**	23
5	$[Dy\{Cp(iPr)_4\}_2][B(C_6F_5)_4]$	1848	$3.39\ 10^{-12}$	439	$2.27\ 10^{-5}$	2	19	∞	**21**	60	23
6	$[Dy(OtBu)_2(py)_5][BPh_4]$	1815	$1.17\ 10^{-12}$	—	$1.00\ 10^{-6}$	3.77	12	∞	**12**	57	24
7	$[Dy(Cp^{ttt})_2][B(C_6F_5)_4]$	1760	$1.99\ 10^{-11}$	—	$4.29\ 10^{-6}$	1.88	57	∞	62	**60**	25
8	$[Dy(Dtp)_2][Al\{OC\text{-}(CF_3)_3\}_4]$	1760	$2.00\ 10^{-12}$	—	$3.16\ 10^{-4}$	1.1	24	∞	**23**	56	26
9	$[Tb(Cp^{iPr5})_2]$	1734	$2.46\ 10^{-11}$	642	$9.69\ 10^{-18}$	8.69	53	∞	**53**	60	27
10	$[Dy(L^{N6})(Ph_3SiO)_2](BPh_4)$	1124	$1.52\ 10^{-11}$	0.016	0.014	2.95	—	**0**	1	38	28
11	$[Dy(L^{N6})(Ph_3SiO)_2](PF_6)$	1080	$1.96\ 10^{-11}$	0.025	0.34	2.32	—	**0**	0	37	28
12	$[Dy(L^{N6})(2,4\text{-di-tBu-PhO})_2](PF_6)$	973	$3.17\ 10^{-12}$	0.003	0.37	2.5	—	**0**	0	31	28
13	$[Dy(OtBu)Cl(THF)_5][BPh_4]$	950	$3.00\ 10^{-12}$	1.4	$2.10\ 10^{-6}$	4.6	—	**0**	6	31	7
14	$[Dy(bbpen)(tpo)_2][BPh_4]$	944	$1.73\ 10^{-12}$	0.64	$3.88\ 10^{-4}$	3.69	—	**0**	2	30	29
15	$[DyIm^{Dipp}NCl_2(THF)_3]$	803	$1.4\ 10^{-12}$	—	$8.6\ 10^{-4}$	4	2	∞	**2**	25	30
16	$[(NN^{TBS})DyI(THF)_2]$	771	$8.20\ 10^{-11}$	0.01	0.21	2.24	—	**0**	**0**	28	31
17	$[DyL^{ON3}(C_5H_{10}NS_2)_2]$	638	$2.99\ 10^{-12}$	0.017	0.02	3.24	—	**0**	1	20	32

Table 2 Modification of the blocking temperature (τ = 100 s criterion) by neglection of the Raman term ($T_{B,noR}$)

	Chemical formula	$T_{B,100}$	$T_{B,100,noR}$	ΔT_R
1	$[Dy(Cp(Me)_5)(Cp(iPr)_5)][B(C_6F_5)_4]$	67	72	5
2	$[Dy\{Cp(iPr)_4(Me)\}_2][B(C_6F_5)_4]$	64	69	5
3	$[Dy\{Cp(iPr)_4(Et)\}_2][B(C_6F_5)_4]$	59	66	7
4	$[Dy\{Cp(iPr)_5\}_2][B(C_6F_5)_4]$	65	65	0
5	$[Dy\{Cp(iPr)_4\}_2][B(C_6F_5)_4]$	19	60	41
6	$[Dy(OtBu)_2(py)_5][BPh_4]$	12	57	45
7	$[Dy(Cp^{ttt})_2][B(C_6F_5)_4]$	57	61	4
8	$[Dy(Dtp)_2][Al\{OC\text{-}(CF_3)_3\}_4]$	24	56	32
9	$[Tb(Cp^{iPr5})_2]$	53	60	7
15	$[DyIm^{Dipp}NCl_2(THF)_3]$	2	26	24

nificantly rise the blocking temperature of this group. In sum, the potential of vibrational tuning strategies to improve T_B will depend on the limiting mechanism, which can be easily determined from experimentally adjusted fitting parameters.

Comparing T_{Ra} and T_{Or}, we observe the Raman limiting temperature is normally similar or lower than T_{Or}. A notable exception is complex **4**, where the Raman limiting temperature is 161 K, much higher than the Orbach (65 K). This complex is a highly sterically encumbered dysprosocenium $[Dy\{Cp(iPr)_5\}_2]$ derivative, with a high Cp–Dy–Cp angle of 162.1°. Other derivatives presented in the same study show how chemical functionalization of cyclopentadienyl rings can modify metal–ligand vibrational modes and consequently, vibrational demagnetization parameters.[23]

Among the strategies to suppress Raman relaxation, current proposals point to the identification key vibrational modes with high spin-vibrational coupling,[9,20] ligand stiffening[23] and vibrational detuning.[3] A recent study highlights the importance of suppressing intermolecular interactions to reduce spin-phonon coupling associated with acoustic modes since the low energy region of the phonon spectrum seems to account for a substantial contribution in Raman relaxation.[33]

An example of trends in Raman limited systems is the study of Giansiracusa *et al.*[18] Authors presented an empirical correlation between the relaxation time measured at the switching temperature between Raman and Orbach mechanisms (named τ_{switch}) and the blocking temperature. The correlation is related with Raman contribution to relaxation rate since most blocking temperatures that afford this trend are limited by this mechanism. Comparing τ_{switch} values allows to have a clean comparison of the Raman contribution for each case since the Orbach contribution is equal to the Raman term precisely at this point. Relaxation times at other temperatures will have a non-systematic contribution from the exponential term, spoiling the correlation.

Summing up, we observe that the Orbach limiting temperature (T_{Or}) acts as higher limit for the achievable T_B and is close to it when other relaxation mechanisms are not dominant. For dysprosocenium derivatives (**1–5**, **7**), T_{Or} values span a relatively narrow interval (between 60 K and 72 K), in the range of the observed record blocking temperatures. In this way, T_{Or} itself becomes an interesting parameter for the identification of candidate SMM with high T_B. In the next section, we evaluate the possibility of calculating T_{Or} directly from *ab initio* methods.

Setting the exponential term to be equal to the reference temperature (*e.g.* 100 s). ($\exp(-U_{eff}/T_{Or})/\tau_0 = 1/\tau_{ref}$), the Orbach limiting temperature can be expressed as:

$$T_{Or} = -\frac{U_{eff}}{\ln\left(\frac{\tau_0}{\tau_{ref}}\right)} \quad (3)$$

Recently, we presented a model that provides estimates for the ground and excited-state tunnelling times.[34] In conjunction with *ab initio* state energies, the model was employed to

 This journal is © the Partner Organisations 2020

Published on 01 June 2020. Downloaded on 2/3/2025 9:56:01 AM.

calculate tunnelling relaxation times and non-trivial demagnetization pathways for high-performance SMMs. The same information can be used to derive meaningful Orbach limiting temperature values. Ten complexes from Table 1 were selected for calculations, which molecular structures are presented in Fig. 1.

To check if thermally assisted tunnelling relaxation is properly accounted, we calculated the effective demagnetization pathways for all complexes based on our recent model.[34] In a nutshell, the effective demagnetization barrier is defined considering all state energies and their contributions to the tunnelling rate, following the equation:

$$U_{\mathrm{eff}}(T) = \sum_{i=1}^{M} \frac{k_i(T)}{k_{\mathrm{tot}}(T)} E_i \qquad (4)$$

where M is the number of Kramers' doublets, $k_{\mathrm{tot}}(T)$ and $k_{\mathrm{i}}(T)$ are the total relaxation rate and the rate of state i, respectively and E_{i} is the energy of state i. At very low temperature, only the ground state is populated and $U_{\mathrm{eff}} = 0$. At higher temperatures, excited states will have a larger contribution to the total rate, U_{eff} will rise and reach a plateau representing the effective demagnetization barrier consistent with the Arrhenius law. Fig. 2 presents calculated effective barriers for two contrasting cases: (i) complex **1**, which shows two excited states contributing to the barrier where the dominant is the fifth excited doublet (1919 K) and the secondary is the fourth excited state (1676 K). Remaining states do not contribute significantly, yielding U_{eff} = 1893 K (see Fig. 2 left). This value is reasonably close, although a bit lower than the experimental barrier (2217 K). (ii) Complex **17** has the lowest barrier of the group (638 K). CASSCF calculations are in nice agreement with

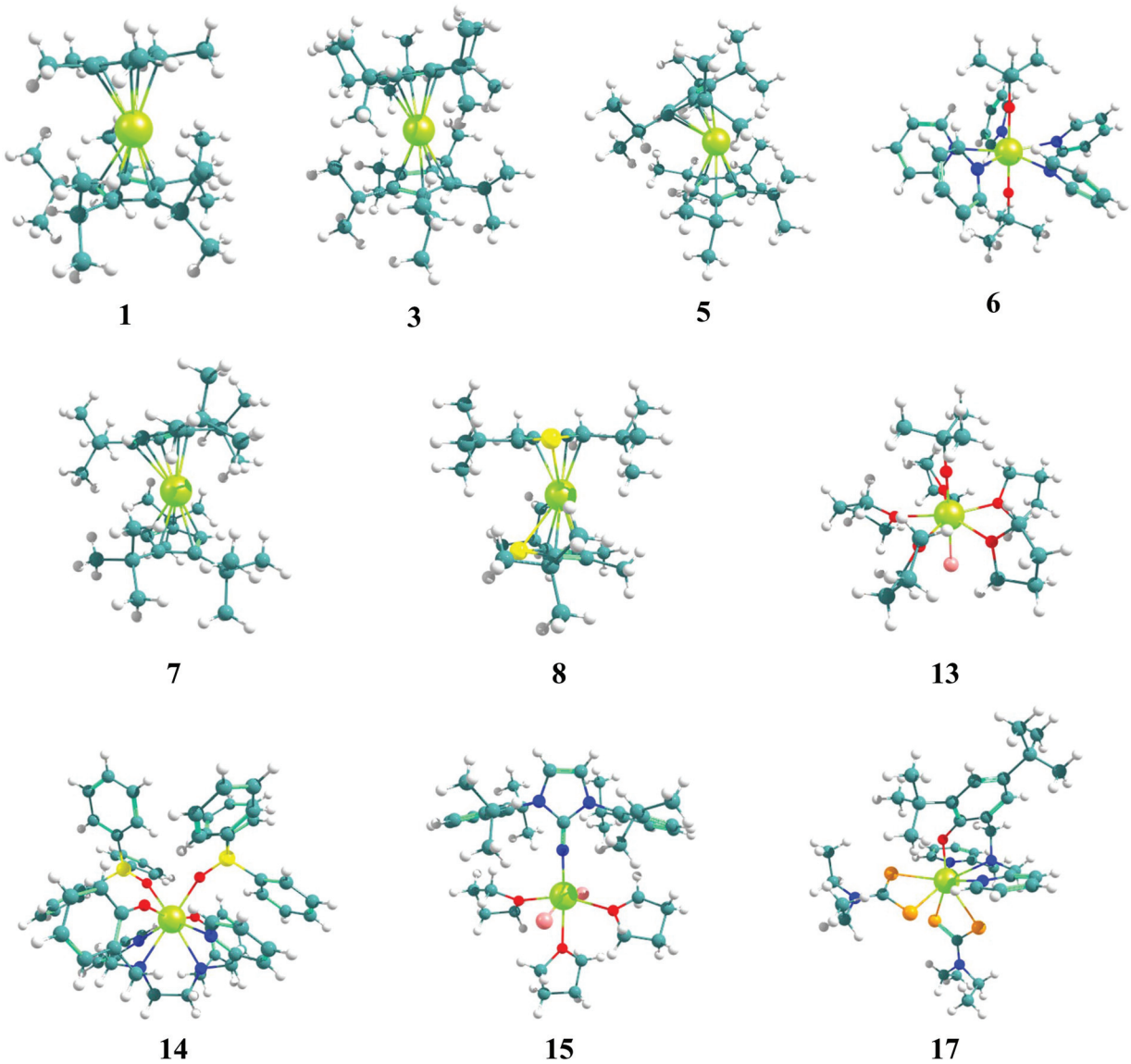

Fig. 1 Molecular structures for CASSCF calculations. Colour code: green (Dy), Cl (pink), S (orange), P (yellow), O (red), N (blue), C (grey), H (white).

Published on 01 June 2020. Downloaded on 2/3/2025 9:56:01 AM.

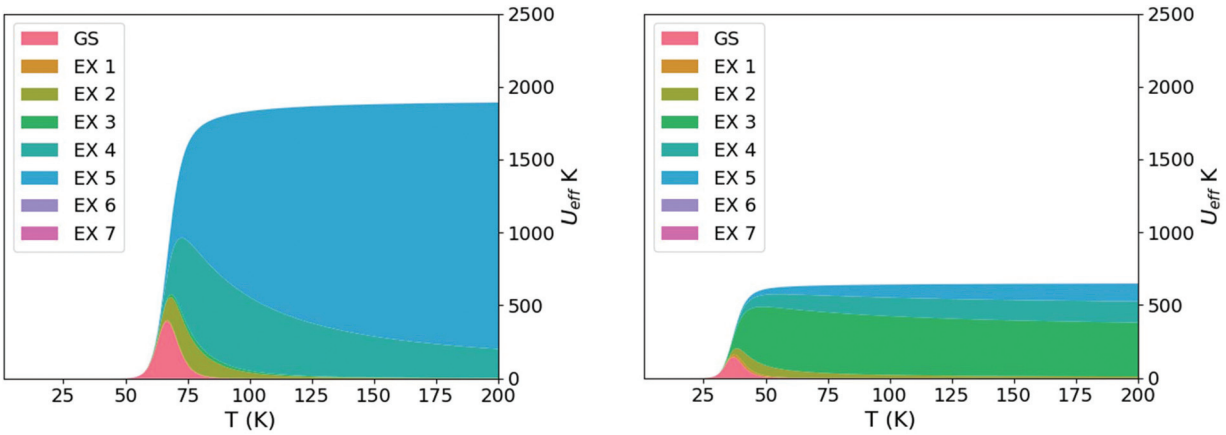

Fig. 2 Effective demagnetization barrier including relative contributions from the ground state (GS) and seven lowest excited states (EX *n*). For **1** (left) and **17** (right).

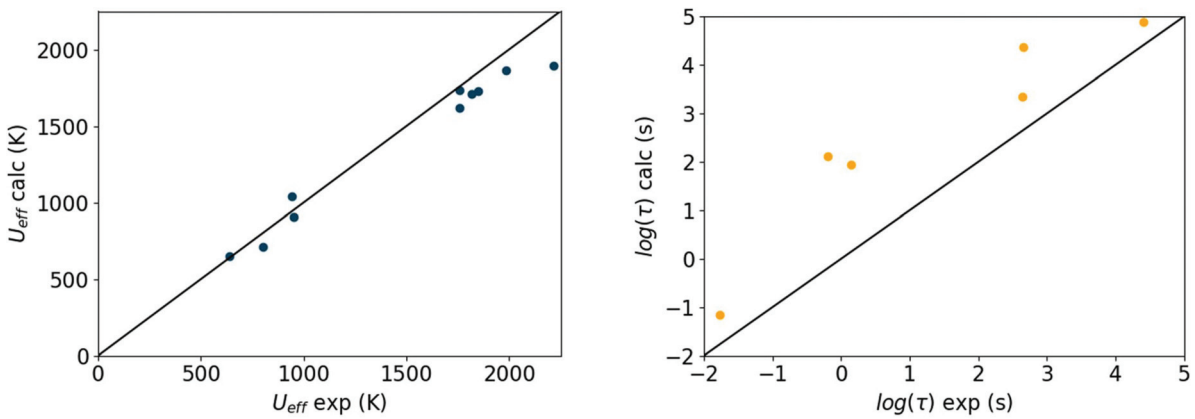

Fig. 3 Relation between experimental and calculated effective demagnetization barriers (left) and ground state tunnelling times (right). Data for these plots is available in Table S2.†

experiment (649 K) and predict the participation of three excited states at 626 K, 668 K and 707 K in thermally assisted quantum tunnelling. Remaining demagnetization pathway calculations are presented in Fig. S1.†

For all cases, calculated barriers agree with experiment (see Fig. 3, left and Table S2†), confirming the adequacy of this methodology to account for thermally assisted tunnelling demagnetization in the studied systems. Regarding ground state tunnelling relaxation times, Fig. 3, right shows the correlation between experimental and calculated values, where *ab initio* relaxation times tend to be systematically slower than experiment. This bias was already observed for systems with relatively slow tunnelling times[34] and might be related to the neglection of other sources of tunnelling demagnetization beyond interelectronic dipolar coupling. Despite this bias, the agreement between theory and experiment is satisfactory.

Having confirmed the accuracy of the method for the calculation of U_{eff}, we now focus on τ_0. From modern approaches

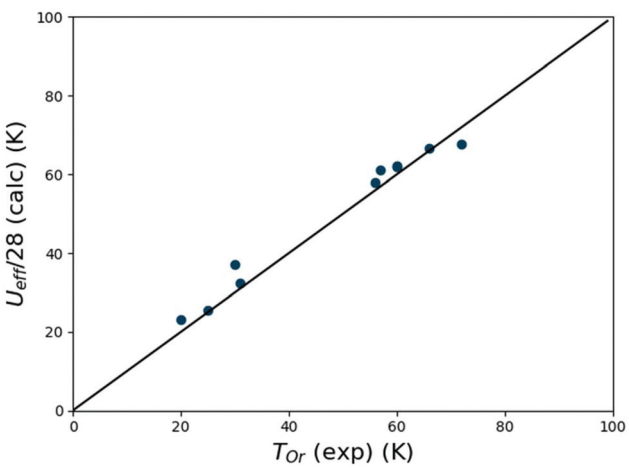

Fig. 4 Relation between the CASSCF calculated U_{eff} and experimental T_{Or}. U_{eff} is divided by 28 to account for the Orbach prefactor τ_0.

 This journal is © the Partner Organisations 2020

Published on 01 June 2020. Downloaded on 2/3/2025 9:56:01 AM.

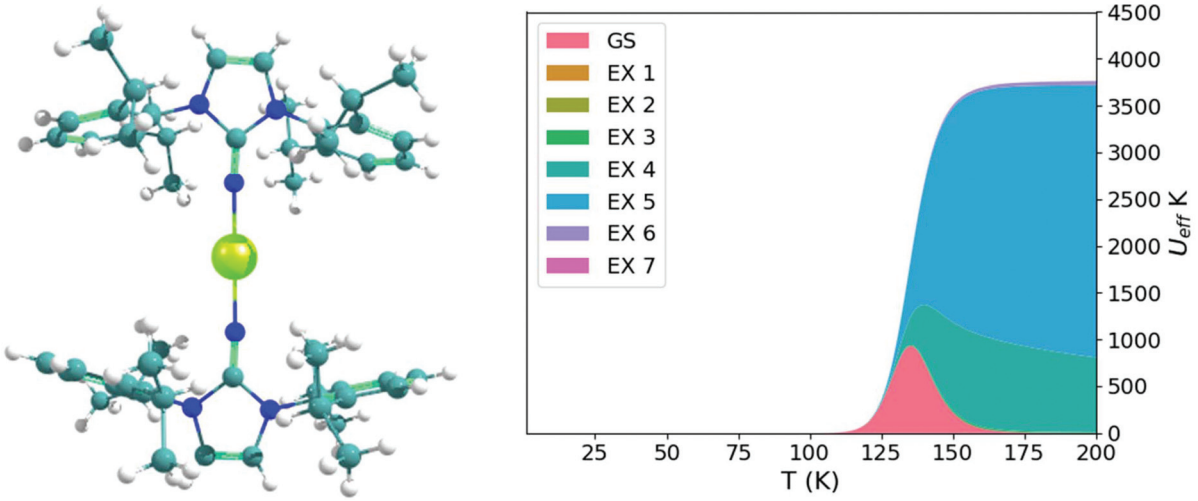

Fig. 5 Left: Molecular structure of the hypothetical diimido-Dy SMM. Color code: green (Dy), blue (N), grey (C), white (H). Right: effective demagnetization barrier including relative contributions from the ground state (GS) and seven lowest excited states (EX *n*). For the proposed diimido complex.

aiming for the theoretical prediction of relaxation times,[3,4,9,20,25,35] τ_0 must be the result of a potentially complex relaxation dynamics governed by the corresponding Master Equation. From a mechanistic point of view, τ_0 will be affected by state mixing given by spin-phonon coupling and by energy exchange with the environment. In principle, current efforts in the direction of suppressing vibration mediated relaxation could also have a positive impact on enhancing τ_0 since both phenomena should depend on similar factors. A deeper understanding of the factors determining τ_0 is an interesting open challenge in this field.

Under this perspective, the accurate prediction of τ_0 seems like an extremely complicated task. Fortunately, we only require a rough estimation of this parameter to obtain decent theoretical values for T_{Or} due to the logarithmic dependence of eqn (3) with respect to τ_0. From typical τ_0 values ranging from 10^{-11}–10^{-12} s and τ_{ref} = 100 s, the denominator of eqn (3) will be around 28. This number can serve as a rule of thumb for the U_{eff}/T_{Or} ratio and explains the contrast between current record U_{eff} (*circa* 2000 K) and T_B (around 70 K) as 2000/70 = 28.6. Reasonably similar U_{eff}/T_{Or} ratios have been employed in literature to estimate potential blocking temperatures from effective barriers.[36] Fig. 4 shows the relation between an estimation of T_{Or} obtained from the CASSCF U_{eff} divided by 28 and T_{Or} calculated from experimentally fitted U_{eff} and τ_0. Expectedly, the agreement is satisfactory since the calculated barriers are accurate and the Orbach prefactors do not vary much among the studied systems.

Finally, a recent proposal for a high performance SMMs is analysed in terms of its potential blocking temperature. Liu *et al.*[30] synthesized complex **15**, which combines an imido ligand with a very short Dy–N distance (2.12 Å), chlorine and THF ligands. This complex has a relatively high blocking barrier of 803 K despite having a weak ligand (THF) along the highly repulsive axis determined by the imido ligand. Authors propose the diimido ligand as a candidate for a high performance SMM with U_{eff} > 4000 K, according to CASSCF calculations. To check the potential of this hypothetic complex under the framework of this paper, a model structure for the diimido candidate was constructed by replicating the crystallographic geometry of the imido ligand of **15** through a centre of inversion at the Dy position. In this way, calculations were performed on a system with perfect C_i symmetry. In reality, the positive charge of the complex will require the crystallization of a counter anion and some distortion is expected, as in the case of dysprosocenium systems. In any case, the idealized model should be adequate for an approximate estimation of the potential of a diimido SMM. Fig. 5 shows the demagnetization pathway plot for this complex. The calculated effective barrier is 3761 K, dominated by the fifth excited state at 3814 K and a minor contribution of the fourth state at 3570 K. Thus, the Orbach limiting temperature should be around 134 K. This number must be interpreted as an upper limit for the blocking temperature since Raman relaxation is wholly neglected and can lower T_B significantly. Despite this caution, this complex looks promising since its Orbach limiting temperature is 60 K higher than the typical values for dysprosocenium derivatives.

Conclusions

There is no predominant relaxation mechanism determining the τ = 100 s blocking temperature for current high barrier SMMs, as tunnelling, Raman and Orbach limited examples were found in the studied molecule set. However, blocking temperatures for molecules with $T_{B,100}$ > 50 K are mainly limited by the Orbach mechanism. For these systems, Raman relaxation suppression will improve $T_{B,100}$ only modestly. In this way, it is advisable to focus on U_{eff} tuning for this group.

Published on 01 June 2020. Downloaded on 2/3/2025 9:56:01 AM.

Raman limited molecules can benefit from chemical tuning oriented towards vibrational suppression, as their blocking temperatures are expected to increase up to 40 K. However, they are not expected to surpass current record $T_{B,100}$ values. CASSCF calculations provide accurate estimates for the Orbach limiting temperature, providing a higher limit for the achievable blocking temperature. The presented framework can be employed to spot candidate molecules for high $T_{B,100}$ SMMs for both real and hypothetical systems.

Methods

All *ab initio* calculations were performed using the ORCA 4 software.[37] To obtain an accurate representation of the magnetic anisotropy of lanthanide complexes, we selected the CASSCF + QDPT method. This approach is the standard computational procedure to model monometallic SMMs since it allows for inclusion of spin–orbit coupling interaction between multireference wave functions. In a nutshell, the CASSCF + QDPT method has two steps: (i) A CASSCF calculation[38] to converge spin-free wave functions, normally accounting for scalar relativistic effects described by the DKH2 Hamiltonian[39,40] and (ii) the QDPT step, where the spin-free wave functions serve as basis of a state interaction matrix for the spin–orbit coupling operator. Eigenvalues and eigenvectors of this matrix are the relativistic energies and wave functions. CASSCF active space considered the 4f shell (9 electrons and 7 orbitals) with 21, 224 and 490 sextet, quartet and doublet roots, respectively. Dy basis set was SARC2-QZVP[41] and light elements were described by a recontracted version of the Def2-TZVP basis set.[42] (DKH-Def2-TZVP keyword in ORCA).

For the calculation of tunnelling relaxation times τ_{QT}, we employed a recently proposed model based on spin dipolar relaxation.[34] This methodology was recently implemented in a user friendly software package (named UandTau). The program can be obtained free of charge upon request to the author. A description of the procedure to obtain τ_{QT} and an input example are presented as ESI.† This model considers spin-Hamiltonian parameters from *ab initio* calculations and takes into account the molecule orientation in the crystal with respect to its neighbours. This method allows for the calculation of tunnelling relaxation times for each Kramers' doublet, including ground and excited states. As different Spin-Hamiltonian parameters will characterize each doublet, τ_{QT} values will be different among states. Doublets with faster demagnetization will determine the relaxation pathway of the system. The total relaxation time is the sum of individual τ_{QT} values for each doublet, weighted by their Boltzmann populations at a given temperature.

Conflicts of interest

The authors declare no conflict of interest.

Acknowledgements

D. A. thanks FONDECYT Regular 1170524 for financial support. Y. G. y L. L. thank to National Agency for Research and Development (ANID), PhD Scholarships No. 21170520 and 21180269, respectively. Powered@NLHPC: This research was partially supported by the supercomputing infrastructure of the NLHPC (ECM-02). A. C.-A. thanks Universidad de Santiago de Chile, Usach, Project DICYT code 021942AP-PAP.

References

1 D. Gatteschi and R. Sessoli, Quantum Tunneling of Magnetization and Related Phenomena in Molecular Materials, *Angew. Chem., Int. Ed.*, 2003, **42**, 268–297.
2 R. Sessoli, D. Gatteschi, A. Caneschi and M. A. Novak, Magnetic Bistability in a Metal-Ion Cluster., *Nature*, 1993, **365**, 141–143.
3 L. Escalera-Moreno, J. J. Baldoví, A. Gaita-Ariño and E. Coronado, Spin States, Vibrations and Spin Relaxation in Molecular Nanomagnets and Spin Qubits: A Critical Perspective, *Chem. Sci.*, 2018, **9**, 3265–3275.
4 A. Lunghi, F. Totti, R. Sessoli and S. Sanvito, The Role of Anharmonic Phonons in Under-Barrier Spin Relaxation of Single Molecule Magnets, *Nat. Commun.*, 2017, **8**, 14620.
5 S. Gómez-Coca, A. Urtizberea, E. Cremades, P. J. Alonso, A. Camón, E. Ruiz and F. Luis, Origin of Slow Magnetic Relaxation in Kramers Ions with Non-Uniaxial Anisotropy, *Nat. Commun.*, 2014, **5**, 4300.
6 D. H. Moseley, S. E. Stavretis, K. Thirunavukkuarasu, M. Ozerov, Y. Cheng, L. L. Daemen, J. Ludwig, Z. Lu, D. Smirnov, C. M. Brown, A. Pandey, A. J. Ramirez-Cuesta, A. C. Lamb, M. Atanasov, E. Bill, F. Neese and Z.-L. Xue, Spin–Phonon Couplings in Transition Metal Complexes with Slow Magnetic Relaxation, *Nat. Commun.*, 2018, **9**, 2572.
7 Y. S. Ding, K. X. Yu, D. Reta, F. Ortu, R. E. P. Winpenny, Y. Z. Zheng and N. F. Chilton, Field- and Temperature-Dependent Quantum Tunnelling of the Magnetisation in a Large Barrier Single-Molecule Magnet, *Nat. Commun.*, 2018, **9**, 3134.
8 M. A. Sørensen, U. B. Hansen, M. Perfetti, K. S. Pedersen, E. Bartolomé, G. G. Simeoni, H. Mutka, S. Rols, M. Jeong, I. Zivkovic, M. Retuerto, A. Arauzo, J. Bartolomé, S. Piligkos, H. Weihe, L. H. Doerrer, J. van Slageren, H. M. Rønnow, K. Lefmann and J. Bendix, Chemical Tunnel-Splitting-Engineering in a Dysprosium-Based Molecular Nanomagnet, *Nat. Commun.*, 2018, **9**, 1292.
9 A. Lunghi, F. Totti, S. Sanvito and R. Sessoli, Intra-Molecular Origin of the Spin-Phonon Coupling in Slow-Relaxing Molecular Magnets, *Chem. Sci.*, 2017, **8**, 6051–6059.
10 F. Pointillart, K. Bernot, S. Golhen, B. Le Guennic, T. Guizouarn, L. Ouahab and O. Cador, Magnetic Memory in an Isotopically Enriched and Magnetically Isolated

 This journal is © the Partner Organisations 2020

Published on 01 June 2020. Downloaded on 2/3/2025 9:56:01 AM.

Mononuclear Dysprosium Complex, *Angew. Chem., Int. Ed.*, 2015, **54**, 1504–1507.

11 D. Aravena and E. Ruiz, Shedding Light on the Single-Molecule Magnet Behavior of Mononuclear Dy III Complexes, *Inorg. Chem.*, 2013, **52**, 13770–13778.

12 D. H. Moseley, S. E. Stavretis, Z. Zhu, M. Guo, C. M. Brown, M. Ozerov, Y. Cheng, L. L. Daemen, R. Richardson, G. Knight, K. Thirunavukkuarasu, A. J. Ramirez-Cuesta, J. Tang and Z.-L. Xue, Inter-Kramers Transitions and Spin–Phonon Couplings in a Lanthanide-Based Single-Molecule Magnet, *Inorg. Chem.*, 2020, **59**, 5218–5230.

13 A. Abragam and B. Bleaney, *Electron Paramagnetic Resonance of Transition Ions*, Oxford University Press, Oxford, 1970.

14 G. Velkos, D. S. Krylov, K. Kirkpatrick, L. Spree, V. Dubrovin, B. Büchner, S. M. Avdoshenko, V. Bezmelnitsyn, S. Davis, P. Faust, J. Duchamp, H. C. Dorn and A. A. Popov, High Blocking Temperature of Magnetization and Giant Coercivity in the Azafullerene Tb2@C79N with a Single-Electron Terbium-Terbium Bond, *Angew. Chem., Int. Ed.*, 2019, **58**, 5891–5896.

15 S. Demir, M. I. Gonzalez, L. E. Darago, W. J. Evans and J. R. Long, Giant Coercivity and High Magnetic Blocking Temperatures for N_2^{3-} Radical-Bridged Dilanthanide Complexes upon Ligand Dissociation, *Nat. Commun.*, 2017, **8**, 2144.

16 S. K. Gupta, T. Rajeshkumar, G. Rajaraman and R. Murugavel, An Air-Stable Dy(III) Single-Ion Magnet with High Anisotropy Barrier and Blocking Temperature, *Chem. Sci.*, 2016, **7**, 5181–5191.

17 D. Gatteschi, R. Sessoli and J. Villain, *Molecular Nanomagnets*, Oxford University Press, 2006.

18 M. J. Giansiracusa, A. K. Kostopoulos, D. Collison, R. E. P. Winpenny and N. F. Chilton, Correlating Blocking Temperatures with Relaxation Mechanisms in Monometallic Single-Molecule Magnets with High Energy Barriers (U_{Eff} > 600 K), *Chem. Commun.*, 2019, **55**, 7025–7028.

19 F. Guo, B. M. Day, Y. Chen, M. Tong, A. Mansikkamäki and R. A. Layfield, Magnetic Hysteresis up to 80 Kelvin in a Dysprosium Metallocene Single-Molecule Magnet, *Science*, 2018, **362**, 1400–1403.

20 L. Escalera-Moreno, N. Suaud, A. Gaita-Ariño and E. Coronado, Determining Key Local Vibrations in the Relaxation of Molecular Spin Qubits and Single-Molecule Magnets, *J. Phys. Chem. Lett.*, 2017, **8**, 1695–1700.

21 G. A. Craig, A. Sarkar, C. H. Woodall, M. A. Hay, K. E. R. Marriott, K. V. Kamenev, S. A. Moggach, E. K. Brechin, S. Parsons, G. Rajaraman and M. Murrie, Probing the Origin of the Giant Magnetic Anisotropy in Trigonal Bipyramidal Ni(II) under High Pressure, *Chem. Sci.*, 2018, **9**, 1551–1559.

22 M. S. Norre, C. Gao, S. Dey, S. K. Gupta, A. Borah, R. Murugavel, G. Rajaraman and J. Overgaard, High-Pressure Crystallographic and Magnetic Studies of Pseudo-D_{5h} Symmetric Dy(III) and Ho(III) Single-Molecule Magnets, *Inorg. Chem.*, 2020, **59**, 717–729.

23 K. Randall McClain, C. A. Gould, K. Chakarawet, S. J. Teat, T. J. Groshens, J. R. Long and B. G. Harvey, High-Temperature Magnetic Blocking and Magneto-Structural Correlations in a Series of Dysprosium(III) Metallocenium Single-Molecule Magnets, *Chem. Sci.*, 2018, **9**, 8492–8503.

24 Y.-S. Ding, N. F. Chilton, R. E. P. Winpenny and Y.-Z. Zheng, On Approaching the Limit of Molecular Magnetic Anisotropy: A Near-Perfect Pentagonal Bipyramidal Dysprosium(III) Single-Molecule Magnet, *Angew. Chem., Int. Ed.*, 2016, **55**, 16071–16074.

25 C. A. P. Goodwin, F. Ortu, D. Reta, N. F. Chilton and D. P. Mills, Molecular Magnetic Hysteresis at 60 Kelvin in Dysprosocenium, *Nature*, 2017, **548**, 439–442.

26 P. Evans, D. Reta, G. F. S. Whitehead, N. F. Chilton and D. P. Mills, Bis-Monophospholyl Dysprosium Cation Showing Magnetic Hysteresis at 48 K, *J. Am. Chem. Soc.*, 2019, **141**, 19935–19940.

27 C. A. Gould, K. R. McClain, J. M. Yu, T. J. Groshens, F. Furche, B. G. Harvey and J. R. Long, Synthesis and Magnetism of Neutral, Linear Metallocene Complexes of Terbium(II) and Dysprosium(II), *J. Am. Chem. Soc.*, 2019, **141**, 12967–12973.

28 A. B. Canaj, S. Dey, E. R. Martí, C. Wilson, G. Rajaraman and M. Murrie, Insight into D_{6h} Symmetry: Targeting Strong Axiality in Stable Dysprosium(III) Hexagonal Bipyramidal Single-Ion Magnets, *Angew. Chem.*, 2019, **131**, 14284–14289.

29 S. Bala, G.-Z. Huang, Z.-Y. Ruan, S.-G. Wu, Y. Liu, L.-F. Wang, J.-L. Liu and M.-L. Tong, A Square Antiprism Dysprosium Single-Ion Magnet with an Energy Barrier over 900 K, *Chem. Commun.*, 2019, **55**, 9939–9942.

30 B.-C. Liu, N. Ge, Y.-Q. Zhai, T. Zhang, Y.-S. Ding and Y.-Z. Zheng, An Imido Ligand Significantly Enhances the Effective Energy Barrier of Dysprosium(III) Single-Molecule Magnets, *Chem. Commun.*, 2019, **55**, 9355–9358.

31 K. L. M. Harriman, J. L. Brosmer, L. Ungur, P. L. Diaconescu and M. Murugesu, Pursuit of Record Breaking Energy Barriers: A Study of Magnetic Axiality in Diamide Ligated Dy^{III} Single-Molecule Magnets, *J. Am. Chem. Soc.*, 2017, **139**, 1420–1423.

32 A. B. Canaj, S. Dey, O. Céspedes, C. Wilson, G. Rajaraman and M. Murrie, There Is Nothing Wrong with Being Soft: Using Sulfur Ligands to Increase Axiality in a Dy(III) Single-Ion Magnet, *Chem. Commun.*, 2020, **56**, 1533–1536.

33 A. Chiesa, F. Cugini, R. Hussain, E. Macaluso, G. Allodi, E. Garlatti, M. Giansiracusa, C. A. P. Goodwin, F. Ortu, D. Reta, J. M. Skelton, T. Guidi, P. Santini, M. Solzi, R. De Renzi, D. P. Mills, N. F. Chilton and S. Carretta, Understanding Magnetic Relaxation in Single-Ion Magnets with High Blocking Temperature, *Phys. Rev. B*, 2020, **101**, 174402.

34 D. Aravena, Ab Initio Prediction of Tunneling Relaxation Times and Effective Demagnetization Barriers in Kramers

Lanthanide Single-Molecule Magnets, *J. Phys. Chem. Lett.*, 2018, **9**, 5327–5333.
35 M. Atanasov, D. Aravena, E. Suturina, E. Bill, D. Maganas and F. Neese, First Principles Approach to the Electronic Structure, Magnetic Anisotropy and Spin Relaxation in Mononuclear 3d-Transition Metal Single Molecule Magnets, *Coord. Chem. Rev.*, 2015, **289–290**, 177–214.
36 N. F. Chilton, C. A. P. Goodwin, D. P. Mills and R. E. P. Winpenny, The First Near-Linear Bis(Amide) f-Block Complex: A Blueprint for a High Temperature Single Molecule Magnet, *Chem. Commun.*, 2015, **51**, 101–103.
37 F. Neese, Software Update: The ORCA Program System, Version 4.0., *Wiley Interdiscip. Rev.: Comput. Mol. Sci.*, 2018, **8**, e1327.
38 P.-Å. Malmqvist and B. O. Roos, The CASSCF State Interaction Method, *Chem. Phys. Lett.*, 1989, **155**, 189–194.
39 N. Rösch, S. Krüger, M. Mayer and V. A. Nasluzov, The Douglas-Kroll-Hess Approach to Relativistic Density Functional Theory: Methodological Aspects and Applications to Metal Complexes and Clusters, in *Recent Developments and Applications of Modern Density Functional Theory*, ed. J. Seminario, Elsevier, 1996, vol. 4, pp. 497–566.
40 T. Nakajima and K. Hirao, The Douglas–Kroll–Hess Approach, *Chem. Rev.*, 2012, **112**, 385–402.
41 D. Aravena, F. Neese and D. A. Pantazis, Improved Segmented All-Electron Relativistically Contracted Basis Sets for the Lanthanides, *J. Chem. Theory Comput.*, 2016, **12**, 1148–1156.
42 F. Weigend and R. Ahlrichs, Balanced Basis Sets of Split Valence, Triple Zeta Valence and Quadruple Zeta Valence Quality for H to Rn: Design and Assessment of Accuracy, *Phys. Chem. Chem. Phys.*, 2005, **7**, 3297–3305.

Published on 01 June 2020. Downloaded on 2/3/2025 9:56:01 AM.

This journal is © the Partner Organisations 2020